

Parallel Microcracks-based Ultrasensitive and Highly Stretchable Strain Sensors

Morteza Amjadi,^{*,†} Mehmet Turan,[†] Cameron P. Clementson,^{†,‡} and Metin Sitti^{*,†}

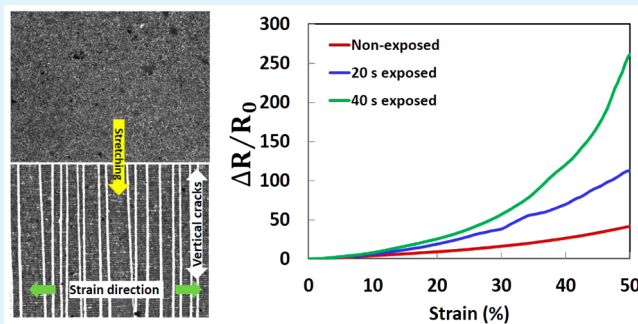
[†]Physical Intelligence Department, Max Planck Institute for Intelligent Systems, Heisenberstr. 3, 70569, Stuttgart, Germany

[‡]Department of Biomedical Engineering, University of Arizona, Tucson 85721, Arizona, United States

Supporting Information

ABSTRACT: There is an increasing demand for flexible, skin-attachable, and wearable strain sensors due to their various potential applications. However, achieving strain sensors with both high sensitivity and high stretchability is still a grand challenge. Here, we propose highly sensitive and stretchable strain sensors based on the reversible microcrack formation in composite thin films. Controllable parallel microcracks are generated in graphite thin films coated on elastomer films. Sensors made of graphite thin films with short microcracks possess high gauge factors (maximum value of 522.6) and stretchability ($\epsilon \geq 50\%$), whereas sensors with long microcracks show ultrahigh sensitivity (maximum value of 11 344) with limited stretchability ($\epsilon \leq 50\%$). We demonstrate the high performance strain sensing of our sensors in both small and large strain sensing applications such as human physiological activity recognition, human body large motion capturing, vibration detection, pressure sensing, and soft robotics.

KEYWORDS: strain sensors, skin-attachable sensors, wearable sensors, parallel microcracks, human motion detection



INTRODUCTION

Various flexible electronic devices such as stretchable conductors and transparent electrodes,^{1–4} flexible thin film heaters,⁵ flexible nanogenerators,⁶ and soft sensors^{7–10} are being developed due to their facile interaction with human body. In particular, flexible, skin-attachable, and wearable strain sensors are of paramount importance for several applications such as personalized health-monitoring,^{11,12} human or animal motion detection,^{7,13} soft robotics,^{14,15} human–machine interfaces,^{16,17} and beyond. Skin-attachable and wearable strain sensors should be highly flexible, stretchable ($\epsilon \geq 50\%$), and soft to mimic the complex and large degrees of freedom deformations and movements of human skin and clothing.¹⁸ Additionally, strain sensors, as in the case of personalized health-care devices, must possess sufficiently high sensitivity or gauge factor (GF), enabling strain sensors to detect gentle skin strains ($\epsilon \leq 1\%$) induced by blood flow pulse, respiration, and so on.^{10,12,19,20} Continuous monitoring of such signals may significantly improve health conditions and medication quality.^{11,18} On the other hand, highly stretchable and soft strain sensors would be beneficial in soft robotics as feedback controllers for locomotion of soft-bodied robots as well as robotic soft sensory skins, allowing soft robots to sense the surrounding environment.^{10,15,21}

Different mechanisms such as geometrical effect, disconnection between adjacent elements, tunneling effect, and recently crack generation in thin films have been pursued to change the resistance of strain sensors by the external strain.^{7,8,10,12,22}

Highly stretchable strain sensors were demonstrated by composites of carbon nanotubes,^{8,13} nanowires,^{7,9,16} graphene,^{19,23} and hybrid materials and structures.^{20,21,24,25} However, stretchable strain sensors typically showed low sensitivity with high hysteresis behavior and were often unable to detect small strains.^{7,19} Sensitivity of strain sensors was considerably improved by cracked thin film structures, while sensors showed low stretchability ($\epsilon \leq 30\%$) with a highly nonlinear response.^{22,26,27} For example, an ultrahigh sensitive (GFs ~ 2000) strain sensor was reported based on the zip-like nanocrack formation in the brittle platinum thin film deposited on top of polymer layers, while its stretchability was limited only to 2%, far behind the stretchability requirement of skin-mountable and wearable sensors.²² Stretchability of cracks based strain sensors has recently been improved by the microcrack generation in the thickness gradient thin film design ($\epsilon \geq 100\%$).¹² The GFs of the sensor, however, decreased from 161 to 0.58 when it was only stretched to 15%, showing large sensitivity deviations in the strain measurement range. Despite promising results, the development of highly sensitive and highly stretchable strain sensors capable of measuring both small ($\epsilon \leq 1\%$) and large strains ($\epsilon \geq 50\%$) still remains a grand challenge.¹⁰

Received: December 23, 2015

Accepted: February 4, 2016

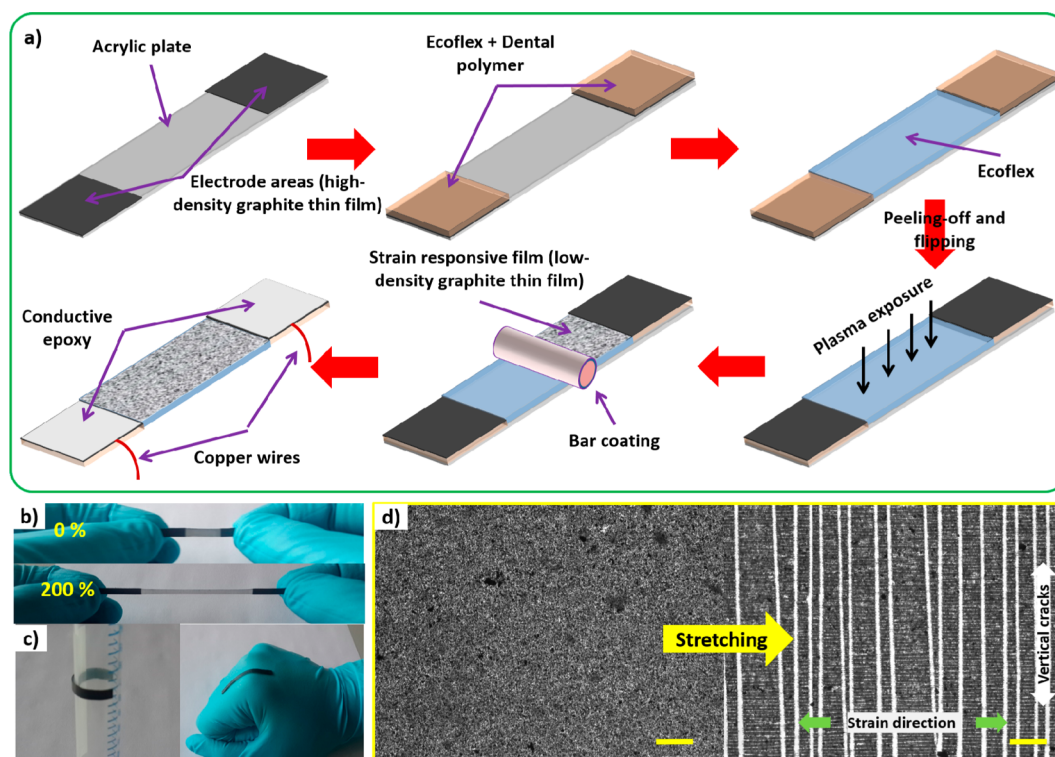


Figure 1. Fabrication process and sample images of the parallel microcrack based highly sensitive and stretchable strain sensors. (a) Fabrication process of the parallel microcrack based flexible strain sensors. (b) Photograph of a strain sensor sample at original length and 200% of stretching. (c) Conformal attachment demonstration of the strain sensors to curvilinear and complex surfaces such as cylindrical tubing and hand finger's base joint surface. (d) Optical microscope images of the graphite thin film coated on an exposed elastomer film before and after microcrack generation; parallel microcrack opening in perpendicular direction of strain. Scale bar: 100 μm .

Herein, we present highly sensitive and stretchable strain sensors through a simple, cost-effective, and mass-producible strategy. High performance strain sensors are developed by controllable introduction of self-organized parallel microcracks in the graphite thin films coated on top of soft elastomer films. The length, width, density, and cracked-area of microcracks are controlled through plasma-exposure and straining parameters, allowing the development of sensors with tunable strain sensing performances. The strain sensors can simultaneously detect deformations from 0.1% to more than 50% with high sensitivity, high stretchability, low hysteresis behavior, and fast response time. They also respond to compressive strains with high sensitivity and good dynamic performance. We show the advantages of our strain sensors in various applications ranges from human motion capturing to vibration wave detection, pressure sensing, and soft robotics.

RESULT AND DISCUSSION

Figure 1a schematically shows the fabrication process of the parallel microcracks based strain sensors (see [Experimental Section](#) for more details). The strain sensors were composed of strain responsive films, flanked by flexible electrodes. Strain responsive films were made of low-density microcracked graphite thin films (around 5 μm thin film thickness) bar coated on Ecoflex elastomer films. The electrodes were fabricated by embedding high-density graphite thin films on the surface of a polymer obtained from a mixture of Ecoflex elastomer and dental polymer, making the electrode sections stiffer than bare Ecoflex in the sensing region (Figure S1, [Supporting Information](#)). This gradient stiffness feature minimized the harmful stress in the electrode areas while

induced maximum strain in the sensing part. The resulting strain sensors were highly stretchable and robust and could easily be attached onto curvilinear surfaces or directly placed on the human skin (Figure 1b,c).

Parallel microcracks were generated and controlled in graphite thin films by the oxygen plasma-exposure of the Ecoflex elastomer films, prior to bar coating of the graphite thin films, and then stretching them from both ends with a controlled strain (Figure 1d). There was no crack formation in the graphite thin film coated on a nonexposed elastomer film under various strains from 0 to 150% (Figure S2 and [Movie S1](#)). Graphite flakes were firmly adhered on the top surface of Ecoflex elastomer without any sliding of flakes or delamination of thin films during stretching. Self-organized parallel microcracks were uniformly initiated in graphite thin films coated on plasma-exposed elastomer films (Figure S2 and [Movie S1](#)). When stretched to 100%, low density and small microcracks (length $\sim 130 \pm 45 \mu\text{m}$ and width $\sim 14.7 \pm 2.3 \mu\text{m}$) were formed in the graphite thin film coated on the 50 s plasma-exposed elastomer film (Figure S3a). The length, width, and density of microcracks were increased when the sample was further stretched (Figure S3). Furthermore, length and width of the microcracks were increased by increase of the exposure time (Figure S3a). Long parallel microcracks were uniformly formed across the entire width of the graphite thin films coated on the 100 and 150 s plasma-exposed elastomer films under 100% strain (Figure S2). In addition, parallel microcracks in the graphite thin films could be created on selected areas by the local plasma-exposure of elastomer films using a mask (Figure S4). The region-controlled formation of microcracks in our method is advantageous over previously reported microcracked

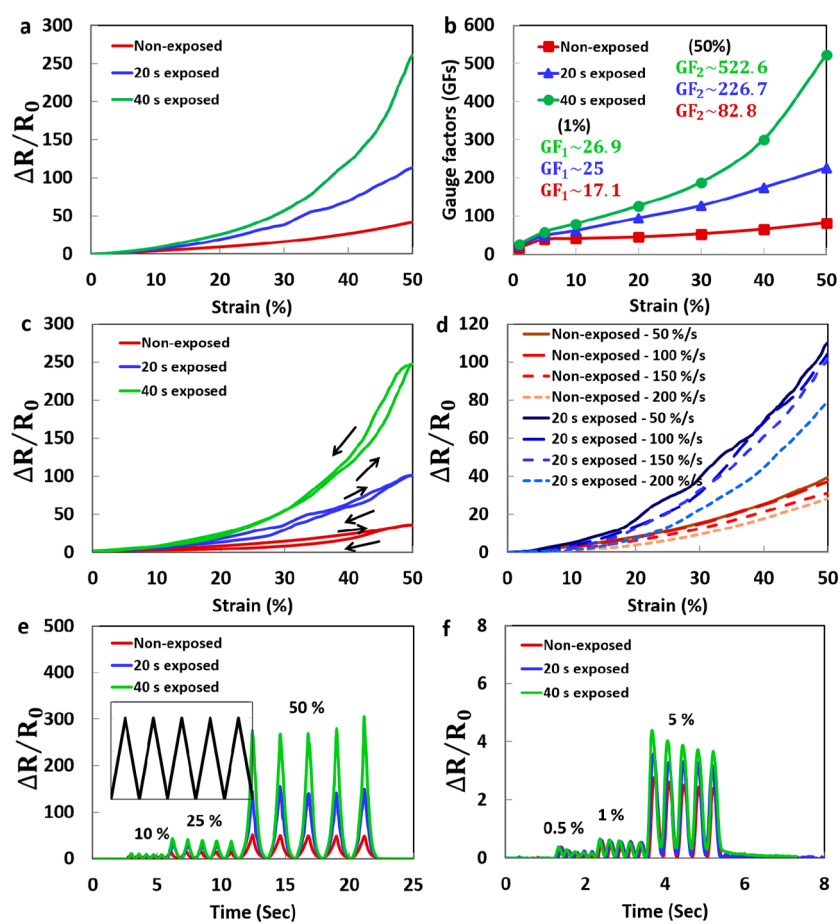


Figure 2. Strain sensing performance of the nonexposed and exposed strain sensors. (a) Piezoresistivity of the nonexposed and oxygen-plasma exposed (20 and 40 s) sensors as a function of the applied axial strain. (b) Gauge factors of the strain sensors as a function of the applied strain. (c) Hysteresis performance of the nonexposed and exposed sensors (strain rate: 50%/s). (d) Effect of the strain rate on the piezoresistivity of the nonexposed and exposed sensors. (e, f) Dynamic response of the nonexposed and exposed sensors to stepwise loading/unloading cycles (5 cycles per each) with large and small strains, respectively.

thin films where microcracks were initiated throughout the thin films with an uncontrollable manner.^{12,13,22,26} Although guided fracture of thin films was demonstrated by sophisticated design of opposing micronotch features,^{28,29} our method is simple and can be applied for the large area fabrication. These uniform parallel microcrack thin films could also be utilized for micro/nanofabrication, biotechnology, photonics, and electronics.^{28,30}

To understand the mechanics behind the parallel microcrack formation in the graphite thin films, we first imaged the surface topography of the nonexposed and exposed Ecoflex elastomer films during stretching, without graphite thin film coating. There was no change in the surface morphology of the nonexposed elastomer film when it was stretched to 100% (Movie S2). On the contrary, perpendicular microgrooves appeared on the top surface of the exposed elastomers during stretching while their surface was smooth beforehand (Movie S2). Longer exposure time led to larger and denser microgroove formations on the surface of the exposed elastomer films. The microgroove features were then disappeared on the surface of the exposed elastomers when they were completely released from the tensile strain and their surface morphology was physically recovered to its original smooth state (Movie S2). To further verify the presence of microgrooves, the depth profile of plasma-exposed surfaces was imaged by a 3D laser scanning confocal microscope. Valley-like structures were

opened on the surface of the exposed elastomers under stretching (Figure S5a,b). Self-organized microgrooves in exposed elastomers were possibly generated by formation of stiffer oxidized polymer layers on the top surface of soft elastomers due to the plasma exposure.^{30–32} We then imaged the surface topology of the exposed elastomer films when graphite thin films were coated on the top. The depth profile of the graphite thin films proved that microcracks in graphite thin films were initiated in the polymer microgroove edges due to localized deformation and stress concentration (Figure S5c,d). Moreover, parallel microcracks were generated through stress transfer from exposed polymer substrates to graphite thin films, different from random microcrack propagation in brittle thin films coated on flexible supports due to the presence of voids or stress concentrated areas in the thin films themselves.^{12,26,30,33} Therefore, length, width, density, and direction of microcracks could be controlled through local plasma-exposure of elastomer films and appropriate choice of straining parameters.

To characterize the strain sensing performance, all samples were first stretched to 100% and then released to allow microcrack formation throughout the graphite thin films coated on the plasma-exposed elastomer films. Hereafter, we refer this 100% stretching and releasing cycle as critical straining. Graphite thin films, coated on elastomer films that were plasma-exposed more than 60 s, were not suitable for the highly

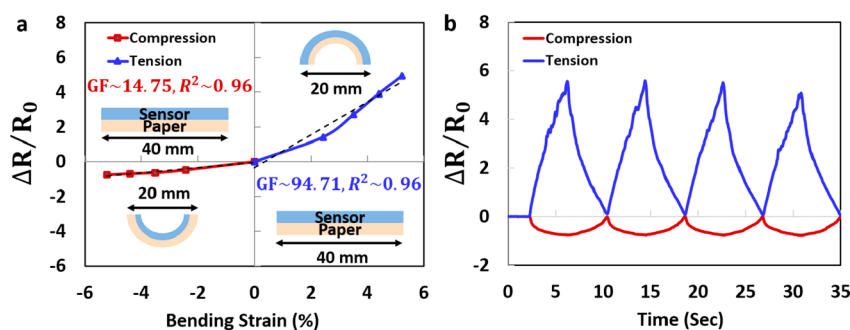


Figure 3. Bending strain measurement of a 40 s exposed strain sensor. (a) Response of the sensor to outward and inward bending. (b) Reversible response of the sensor to the cyclic bending loading.

stretchable strain sensing because electrical connection was lost at small strains due to the rapid and long parallel microcrack opening across the entire width of thin films. In this regard, we limited our exposure time up to 60 s to ensure high stretchability of the graphite thin films. Upon stretching, the resistance of the nonexposed strain sensor (initial resistance ~ 202 k Ω) was almost increased linearly ($R^2 \sim 0.95$) (Figure 2a). The GF (relative change of the resistance versus applied strain; $GF = \Delta R/R_0 \epsilon$) of the sensor was increased from 17.1 to 82.8 when the sensor was stretched from 1 to 50% (Figure 2b). Moreover, the sensor could endure strains as large as 150% with completely reversible electrical properties (Figure S6). The plasma-exposed sensors, however, responded to the applied strain with exponential fashions (Figure 2a). The GFs of the 20 s (initial resistance ~ 304 k Ω) and 40 s (initial resistance ~ 401 k Ω) plasma-exposed sensors were around 25 and 26.9 at 1% strain. Furthermore, the GFs were highly enhanced to about 226.7 and 522.6 when 20 and 40 s plasma-exposed sensors were stretched to 50% (Figure 2b). As shown in Figure 2b, the effect of the plasma-exposure and microcrack generation on the sensitivity improvement of the strain sensors is significant for strains larger than 5%. Ultrahigh GFs ~ 11 300 with stretchability of 50% were achieved for the 60 s plasma-exposed sensor (initial resistance ~ 300 k Ω) by relatively long parallel microcrack opening/closing across the entire width of the graphite thin film, critically limiting the electrical conduction upon stretching (Figure S7). The strain sensing performance of our strain sensors are comparable with recently reported stretchable strain sensors based on the silver nanowires (AgNWs)/polymer (GFs of 2–14 and stretchability of 70%),⁷ fragmentized graphene foam (FGF)/polymer (GFs of 15–29 and stretchability of 70%),²⁰ graphene/rubber (GFs of 10–35 with stretchability of 800%),¹⁹ graphene–nanocellulose nanopaper (GFs of 1.6–7.1 with stretchability of 100%),²¹ and gold nanowires (AuNWs)/rubber (GFs of 6.6–9.9 with stretchability of 350%)¹⁶ composites. A detailed strain sensing performance comparison between our strain sensors and recently reported high performance strain sensors is provided in Table S1.

Further tests were conducted to characterize the dynamic behavior of strain sensors. The sensors exhibited small hysteresis behavior for a constant strain rate of 50%/s, mainly caused by the viscoelastic behavior of Ecoflex films (Figure 2c).⁷ Moreover, the piezoresistive performance of sensors remained almost constant for up to a strain rate of 150%/s, far exceeding the normal strain rate of the human body motions ($\sim 16\%/s$) (Figure 2d).³⁴ The strain sensors retained their performance characteristics under both large and small loading/

unloading cycles (Figure 2e,f). Their electrical resistance was recovered upon complete release of the tensile strain in each cycle. The plasma-exposed sensors exhibited larger resistance changes due to their higher sensitivity and were able to detect 0.1% strain, corresponding to only 10 μm film elongation (Figure S8). Moreover, the strain sensors were capable of measuring strains from 0.1% to more than 50% with high sensitivity and stretchability. In addition, the strain sensors showed durable performance to 2000 cyclic strain tests. The resistance of strain sensors were recorded when the sensors were stretched from 0 to 25% under a fast strain rate of 50%/s (one cycle per second). The electromechanical behavior and GFs of strain sensors remained almost constant without significant changes (Figure S9).

Other than stretching, the performance of sensors was characterized during bending. A 40 s exposed sensor was placed on a hard paper (thickness ~ 100 μm) and outward and inward bending was applied to the paper. Because the strain sensor was much softer than the paper, we assumed that the bending occurred through the neutral axis of the paper. The bending strain of the sensor can then be calculated from $\epsilon = \pm h/r$, where h is the distance of the graphite thin film from the neutral axis of the bent paper (~ 550 μm) and r is the paper radius of curvature. The r value has a relationship with the chord length c as $c = 2r \sin(l/2r)$, where l is the arc length of the paper under bending state.³⁵ Figure 3a illustrates the resistance changes of the sensor versus derived bending strains while the chord length of the paper was decreased from 40 mm to 20 mm under speed of 5 mm/s. The resistance of the sensor was increased under tension and decreased upon compressive strain. Moreover, tensile strain decreased the overlapped area of graphite flakes and increased the resistance. Compressive strain brought flakes closer and consequently reduced the resistance. The GFs of the strain sensor under tension and compression were about 94.71 and 14.75, respectively, with high linearity of 0.96. These values are comparable with the recently reported high performance bending strain sensors.^{35–39} As depicted in Figure 3b, the strain sensor showed high reversible response under both tensile and compressive cyclic loading.

To investigate the reason for performance improvement of the plasma-exposed sensors in microscopic view, the surface morphology of the graphite thin films coated on the nonexposed and exposed elastomer films was monitored under different strains. Because it was hard to track the movement of each flake and interaction between flake–flake junctions under dynamic stretching and releasing cycles, we simulated the repositioning of flakes under stretching condition and visually demonstrated changes in the overlapped areas and

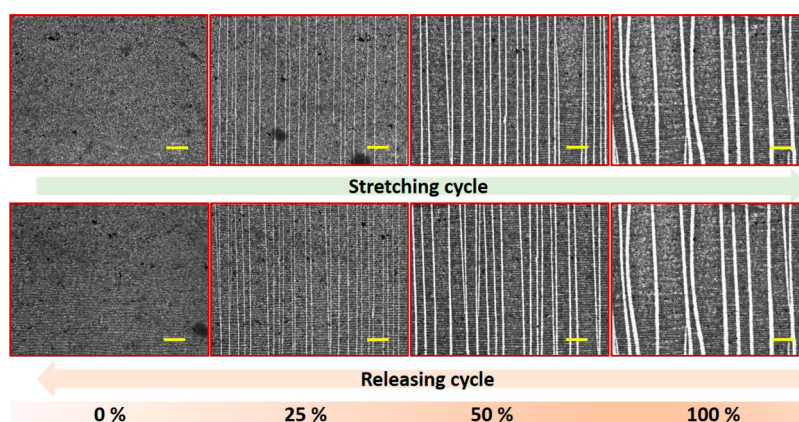


Figure 4. Morphology change of the graphite thin film coated on a 60 s exposed elastomer film under loading/unloading cycle from 0 to 100%. Recovery of the thin film structure after completely release of the sample. Scale bar: 100 μm .

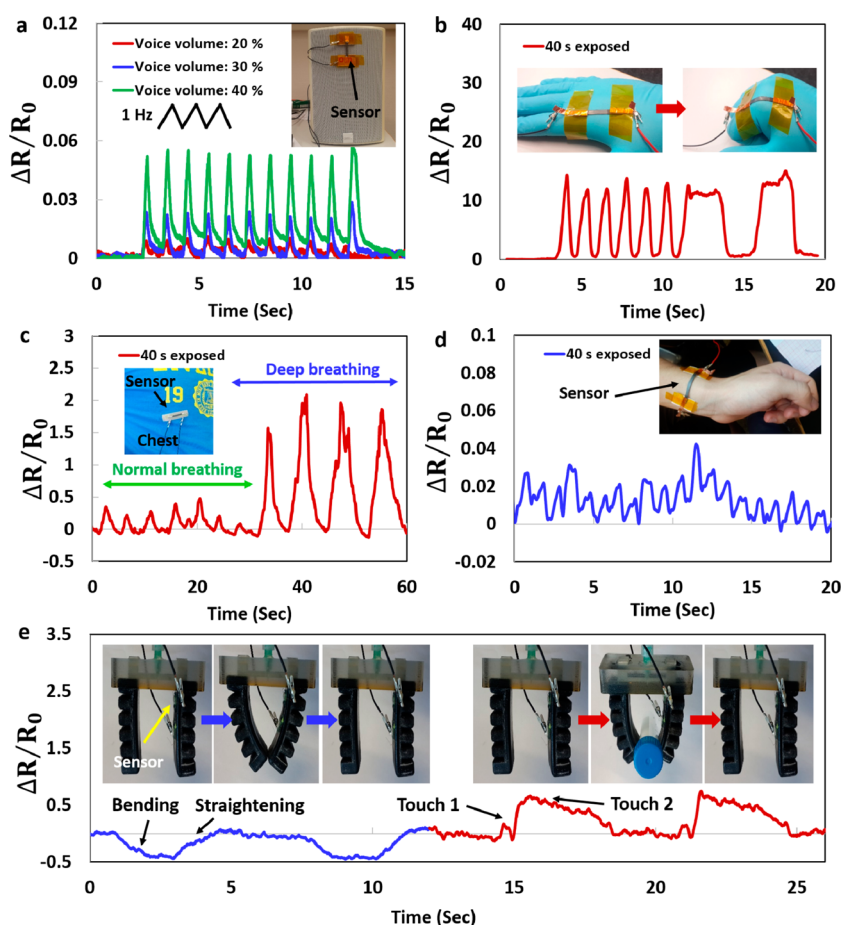


Figure 5. Low-strain and large-strain application demonstrations of the proposed strain sensors. (a) Detection of acoustic waves by a 40 s exposed sensor. (b) Human motion detection by attaching a strain sensor onto a finger joint. (c) Human respiration monitoring when a sensor is placed on clothing in the chest area. (d) Output signal of a sensor when attached to wrist, showing periodic waveform of the blood flow pulse. (e) Integration of the sensors with a two-finger soft robotic gripper. Different responses of the sensor when fingers are closing (bending) and opening (straightening) and then touching, lifting, and releasing an object.

topology of the conductive percolation networks. As shown in Figure S10, at the original length, electrons can pass through overlapped graphite flakes within the percolation network. When the strain sensors were stretched, repositioning of flakes led to smaller overlapped areas and larger interspacing between several overlapped flakes and, thus, lowered the electrical conduction. Larger strains resulted in more disconnection

among graphite flakes, leading to further increase in the electrical resistance. Upon releasing, the graphite flakes were rearranged to their original positions and reconnected, recovering the electrical resistance. We also checked the morphology change of the graphite thin films made of different flake sizes and found more disconnection between conductive chains for thin films made of smaller flake sizes (Figure S10).

We expect to have more sensitive strain sensors with small size flakes, but with lower stretchability since the percolation network can turn nonconductive under smaller strains. Our simulation explains the physical phenomenon behind the piezoresistivity of the crack-free graphite thin films coated on nonexposed elastomers. The surface topography of the graphite thin film coated on the 20 s exposed elastomer film showed large-area graphite thin films wrinkled perpendicular to the stretching direction (Figure S11a). The amplitude of wrinkles was increased by increasing either the exposure time or the strain. Wrinkling of the graphite thin films was likely caused by the surface stiffening of the elastomer film by the plasma exposure.^{28,32} This localized deformation led to larger interspacing and even breakage of the overlapped graphite flakes, making 20 s exposed sensors more sensitive than nonexposed sensors.⁹ When the graphite thin film coated on the 40 s exposed elastomer film was first stretched to the critical strain, short and low density microcracks were emerged in the graphite thin film. Microcracks then disappeared when the composite film was completely released and microcrack edges were connected again. The pregenerated microcracks were opened upon next stretching cycles, resulting in more disconnection between microcrack edges as a function of the applied strain (Movie S1). This repeated opening/closing of microcracks led to reversible electromechanical performance and high sensitivity of strain sensors. Therefore, higher GFs of the 40 s exposed sensors, as compared with nonexposed and 20 s exposed sensors, arose from microcrack formations. When the graphite thin film coated on the 60 s exposed elastomer film was stretched to the critical strain, long parallel microcracks were generated in the entire width of the sample (Movie S1). Moreover, there were only few electrical interconnections between parallel microcracks (Figure S11b,c). Connected junctions were disconnected from each other upon stretching, causing remarkable increase of the resistance. During the releasing cycle, microcrack edges were reconnected, resulting in recovery of the resistance (Figure 4 and Movie S1). We confirmed the significant contribution of microcrack generation on the piezoresistivity of strain sensors by measuring electrical signals of the exposed sensors under strains that did and did not permit microcrack generation (Figure S12).

The high strain sensing performance and high flexibility of our strain sensors enabled us to utilize them for various low-strain and high-strain applications. The strain sensors could detect the vibration waves induced by acoustic-driven and other vibration sources. For example, we placed a two edge-fixed freestanding strain sensor on a speaker and applied sawtooth sound waves with different frequencies (inset of Figure 5a). The strain sensor was able to distinguish sound waves with different sound intensities (Figure 5a). Moreover, the strain sensor responded to sound waves with frequencies up to 14 Hz, showing fast response time of sensors (Figure S13a). For two edge-fixed freestanding polymer films, there are several intrinsic vibrational modes.¹² We increased sound wave frequency from 0 to 150 Hz while measuring the output signal of the strain sensor. As shown in Figure S13b, several resistance peaks appeared at the certain frequencies (i.e., 32, 50, and 99 Hz), showing intrinsic frequency modes of the Ecoflex elastomer film. The data would be of importance for the vibrational analysis of structures and structural health-monitoring.^{40,41} As another trial, we placed a 40 s exposed strain sensor on a mobile phone and measured the response of the sensor when a music track was played by the phone (sound intensity of

around 65 dB) and when the phone was vibrating by a call. The sensor could detect the weak air pressure distributions caused by the music sound and distinguish the vibration patterns with high sensitivity and fast response (Figure S14). In addition, the ability of strain responsive films for pressure sensing was also investigated (Figure S15). Pressure was applied to the two edge-fixed suspended strain responsive films while changes in the electrical resistance were recorded. Suspended films were highly sensitive ($S = \Delta R/R_0 \Delta P \sim 6.6 \text{ kPa}^{-1}$) and could respond to extremely low pressures ($\leq 1 \text{ Pa}$). The attained sensitivity and pressure measurement limit are comparable with recently reported high performance pressure sensors made of the gold NWs/tissue paper composites ($S \sim 1.14 \text{ kPa}^{-1}$ with pressure limit of 13 Pa) and micropylam arrays based pressure sensors ($S \sim 0.55 \text{ kPa}^{-1}$ with pressure limit of 3 Pa).^{42–44}

Our highly soft, sensitive, and stretchable strain sensors can potentially function for full-range human activity recognition, ranging from large human motions like vigorous finger bending and straightening to physiological signals such as heartbeat and breathing. For large-strain applicability of our strain sensors, we attached a 40 s strain sensor onto the figure joint for the human motion detection. We measured the sensor output signal under two conditions: rapid bending–straightening and then bending–holding (about 3 s)–straightening. As illustrated in Figure 5b, the strain sensor responded to both strain conditions with high sensitivity, fast response, and good static and dynamic performances. Human motion detection by the use of skin-mountable and wearable strain sensors can be utilized for sport performance analysis, human-friendly rehabilitation, entertainment technology, and control of slave robots.^{7,8,17,45} As low-strain application attempts, strain sensors were attached onto the clothing in the chest area and wrist for respiration rate and heartbeat monitoring, respectively (insets of Figure 5c,d). As shown in Figure 5c, the strain sensor responded to strains accommodated by the clothing during respiration. Peaks and valleys represent loading and unloading of the strain sensor induced by the extension and shrinkage of the chest area during breathing, respectively. As expected, the signal of the strain sensor was increased under deep breathing condition since larger strains were applied to the sensor. For blood flow pulse monitoring, we placed a 40 s strain sensor on the radial artery in the wrist. The strain sensor could detect tiny skin motions induced by the blood flow pressure. A periodic waveform with frequency of around 1 Hz was recorded from the sensor output signal, within normal heartbeat range of a healthy person.^{19,27} It should be noted that the signal quality of strain sensors can be highly enhanced by the use of adhesive layers between sensors and human skin, e.g. elastomer microfibrillar adhesives^{20,27,43,46–49} or by the design of ultrathin strain sensors. Long-term monitoring of heartbeat and respiration rates, as vital signs, can be potentially applied for the personalized health-monitoring and early diagnosis of diseases.²³

Finally, the strain sensors were implemented on a pneumatically actuated soft robotic gripper as an example of the soft robot demonstration. A strain sensor was mounted in the inner side of the right finger of the gripper for the strain profile monitoring (inset of Figure 5e). After attachment of the sensor, the right finger could still freely bend without any constraints owing to the high flexibility of sensors. We first recorded the output signal of the strain sensor for only bending/straightening of fingers. As illustrated in Figure 5e (blue curve), the resistance of the sensor decreased upon bending of the fingers, showing that compressive strain was accommodated

by the sensor. The resistance of the sensor was recovered to the initial value when the fingers were straightened again. Next, we measured the output signal of the strain sensor when the fingers first touched and then lifted an object. As depicted in the figure (red curve), the signal was first slightly decreased, showing bending of the fingers, prior touching the object. When the right finger touched the object while left finger was not in contact, there was a small peak (touch 1) signal from the sensor. When both fingers contacted to the object, the sensor signal was continuously increased, pointing that right finger experienced tensile strain in the sensor area (touch 2). The signal of the sensor was further increased when we increased the inflation pressure. As a result, touch status, contact force, and bending position of the soft gripper finger could be monitored by the integration of the strain sensor, highlighting the promising applications of our soft strain sensors in soft robotics under both tension and compression. The sensory information could be utilized for the feedback control of the soft robots as well as sensory skin, enabling soft robots to sense their environment and interactive objects.

Our approach for the fabrication of parallel microcracks based strain sensors has several key advancements. First, we used graphite powder as our strain sensing element which is very low-cost, feasibility available, and stable material, comparable with graphene, nanowire, nanotube, and nanoparticle based strain sensors which complex, costly, and time-consuming fabrication processes are needed.^{7,13,26,50} Combining graphite with our mass-producible fabrication process, numerous strain sensors could be fabricated in a simple and low-cost process. Second, graphene flakes were strongly adhered on the surface of elastomer films due to their large surface area.⁵¹ We believe that the interfacial adhesion prosperity between graphite flakes and Ecoflex films plays an important role in the high sensitivity of our strain sensors. Moreover, graphite thin films can undergo substantial structural changes upon stretching without any sliding or delamination. On the other hand, the effect of the possible enhancement of the interfacial adhesion by the plasma-exposure on the performance of strain sensors was found to be negligible (Figure S12). Third, the parallel microcrack generation in this study is novel and different from previously reported cracked thin films which cracks were generated by coating of the brittle thin films on the top of flexible supports.^{12,22,26,27} Here microcrack features were first generated in the polymer substrate as microgrooves and then transferred to the graphite thin films. Therefore, the microcrack formation could be controlled by the surface modification of the polymer substrate before thin film coating. Fourth, our microcracks based strain sensors offering high sensitivity in the whole range of stretchability, enabling high performance strain sensing. In several reported stretchable strain sensors, the sensitivity was very low ($GFs \leq 2$) at small strain levels, making them unsuitable for the low-strain sensing.^{8,21,38} On the other side, sensitivity of several stretchable strain sensors was highly decreased ($GFs \leq 2$) under large strains, limiting their large strain sensing with high sensitivity.^{12,13,23,52} Finally, we believe that the performance of strain sensors could be further improved by changing the thickness of the graphite thin films and localized formation of microcracks. For example, one can couple high sensitivity of the long microcracked films with high stretchability of the crack-free thin films through region-controlled microcrack generation in an optimized geometry.

CONCLUSION

In summary, we present here a simple, cost-effective, and scalable approach for the development of highly sensitive and stretchable strain sensors based on the reversible microcrack formation in the graphite thin films. Strain sensors with high sensitivity ($GFs \geq 100$) and high stretchability ($\epsilon \geq 50\%$) can be achieved by suitable plasma exposure and straining parameters. The strain sensors process stable, reliable, and fast response time to both tensile and compressive strains with very low hysteresis behavior. These sensors can be employed for strain, pressure, and vibration sensing in diverse applications ranging from human physiological activity monitoring to soft robotics.

EXPERIMENTAL SECTION

Preparation of Graphite Solution. Four grams of the graphite powder (averaged flake size $\leq 50 \mu\text{m}$; Merck KGaA) was added to the 100 mL of isopropyl alcohol (IPA). The solution was sonicated for an hour and then stirred for another hour. The well-suspended graphite flakes in IPA was then utilized for spray coating.

Preparation of Graphite Ink. Five grams of the graphite powder was added to 10 mL ethylene glycol (EG), and the mixture was stirred for an hour to fully disperse the graphite flakes in the EG media. The viscous solution was then used for the bar coating of graphite thin films on the top of elastomer films.

Fabrication of Strain Sensors. The fabrication process of the strain sensors is schematically illustrated in Figure 1a. Electrode areas were first patterned on an acrylic plate by polyimide (PI) tape. Then, the graphite solution was air spray (at 2 bar with N_2 gas) coated on the patterned acrylic plate at 70°C . The PI films were then removed from the acrylic plate, leaving high-density graphite thin films in the electrode areas. Next, a mixture of Ecoflex elastomer (Ecoflex 00-30, SMOOTH-ON) and dental polymer (medium flow, Heraeus; 3:1 weight ratio) was poured on the top of the high-density graphite thin films in the electrode areas. After curing the mixed polymer at the room temperature for 30 min, the excess polymer was trimmed away. The space between two end electrodes was then filled with the liquid Ecoflex and cured at 70°C for 2 h. The whole polymer film was then peeled-off from the acrylic plate. The high-density graphite thin films were just buried below the top surface of the mixed polymer due to the penetration of the liquid state polymer into the porous network of the graphite thin films. Next, the Ecoflex elastomer film between two electrodes was exposed to the oxygen plasma (Diener Electronics; power intensity: 0.9) for different time and then the surface of the exposed elastomer was washed with IPA. Low-density graphite thin film was bar coated on the top surface of the nonexposed and exposed elastomer films as strain responsive films. Finally, copper wires were connected to the electrode areas by conductive epoxy (Circuitworks) for electrical measurements.

Electromechanical Tests. The strain sensing tests were conducted by clamping the strain sensors on a motorized moving stage (M-605 High-Accuracy Translation Stage, Physik Instrumente (PI)) and measuring the electrical resistance of the strain sensors with data acquisition (DAQ) system (USB X Series Multifunctional DAQ, National Instruments). The initial resistance of the samples for one time bar coating was around $350 \pm 250 \text{ k}\Omega$. We could achieve much smaller and larger resistance values through the amount of the sprayed solution and the number of coatings. The lateral dimensions of the graphite thin films for strain sensing tests were 30 mm in length (length of the sensing film: 10 mm) and 3 mm in width coated on the 0.5 mm thick elastomer films.

Microscopic Imaging. The surface topology of the nonexposed and exposed strain sensors was tracked by an optical microscope (Microscope Axio Scope.A1, Zeiss). For real-time video capturing, the motorized moving stage was placed in a stereo microscope (SteREO Discovery.V12, Zeiss) and then real-time videos were recorded by a high-speed camera (Grasshopper 3 USB3, PointGrey). The 3D profile

measurements were conducted by a 3D laser scanning confocal microscope (KEYENCE, VK-X200 Series).

Sound Wave Detection. Sawtooth waves with different frequencies were generated by a common audio speaker and controlled by a computer. The sound intensities were approximately measured by a calibrated mobile phone application.

■ ASSOCIATED CONTENT

● Supporting Information

The Supporting Information is available free of charge on the ACS Publications website at DOI: 10.1021/acsami.5b12588.

Stiffness gradient design, microcrack characterization, localized microcrack generation, 3D profile measurement, low-strain sensing, simulation of flake movements, sound visualization, and pressure sensing. (PDF)

(AVI)

(AVI)

■ AUTHOR INFORMATION

Corresponding Authors

*E-mail: sitti@is.mpg.de.

*E-mail: amjadi@is.mpg.de.

Author Contributions

M.A. and M.S. proposed, planned, and supervised the research. M.A. and C.P.C. performed the experiments. M.A. worked on the data analysis. M.T. and M.A. conducted the simulations. M.A. and M.S. wrote the manuscript.

Notes

The authors declare no competing financial interest.

■ ACKNOWLEDGMENTS

The authors thank Kirstin Peterson for prototyping the soft two-finger robot gripper, Dirk Drotlef for the 3D profile imaging, Lindsey Hines for her review and comments, and all other Physical Intelligence Department members for their feedback and comments.

■ REFERENCES

- (1) Lee, P.; Lee, J.; Lee, H.; Yeo, J.; Hong, S.; Nam, K. H.; Lee, D.; Lee, S. S.; Ko, S. H. Highly Stretchable and Highly Conductive Metal Electrode by Very Long Metal Nanowire Percolation Network. *Adv. Mater.* **2012**, *24*, 3326–3332.
- (2) Han, S.; Hong, S.; Ham, J.; Yeo, J.; Lee, J.; Kang, B.; Lee, P.; Kwon, J.; Lee, S. S.; Yang, M. Y. Fast Plasmonic Laser Nanowelding for a Cu-Nanowire Percolation Network for Flexible Transparent Conductors and Stretchable Electronics. *Adv. Mater.* **2014**, *26*, 5808–5814.
- (3) Lee, P.; Ham, J.; Lee, J.; Hong, S.; Han, S.; Suh, Y. D.; Lee, S. E.; Yeo, J.; Lee, S. S.; Lee, D. Highly Stretchable or Transparent Conductor Fabrication by a Hierarchical Multiscale Hybrid Nanocomposite. *Adv. Funct. Mater.* **2014**, *24*, 5671–5678.
- (4) Eom, H.; Lee, J.; Pichitpajongkit, A.; Amjadi, M.; Jeong, J. H.; Lee, E.; Lee, J. Y.; Park, I. Ag@Ni Core-Shell Nanowire Network for Robust Transparent Electrodes against Oxidation and Sulfurization. *Small* **2014**, *10*, 4171–4181.
- (5) Hong, S.; Lee, H.; Lee, J.; Kwon, J.; Han, S.; Suh, Y. D.; Cho, H.; Shin, J.; Yeo, J.; Ko, S. H. Highly Stretchable and Transparent Metal Nanowire Heater for Wearable Electronics Applications. *Adv. Mater.* **2015**, *27*, 4744–4751.
- (6) Jeong, C. K.; Lee, J.; Han, S.; Ryu, J.; Hwang, G. T.; Park, D. Y.; Park, J. H.; Lee, S. S.; Byun, M.; Ko, S. H. A Hyper-Stretchable Elastic-Composite Energy Harvester. *Adv. Mater.* **2015**, *27*, 2866–2875.
- (7) Amjadi, M.; Pichitpajongkit, A.; Lee, S.; Ryu, S.; Park, I. Highly Stretchable and Sensitive Strain Sensor based on Silver Nanowire-Elastomer Nanocomposite. *ACS Nano* **2014**, *8*, 5154–5163.
- (8) Amjadi, M.; Yoon, Y. J.; Park, I. Ultra-Stretchable and Skin-Mountable Strain Sensors using Carbon Nanotubes-Ecoflex Nanocomposites. *Nanotechnology* **2015**, *26*, 375501.
- (9) Kim, K. K.; Hong, S.; Cho, H. M.; Lee, J.; Suh, Y. D.; Ham, J.; Ko, S. H. Highly Sensitive and Stretchable Multidimensional Strain Sensor with Prestrained Anisotropic Metal Nanowire Percolation Networks. *Nano Lett.* **2015**, *15*, 5240–5247.
- (10) Amjadi, M.; Kyung, K.-U.; Park, I.; Sitti, M. Stretchable, Skin-Mountable, and Wearable Strain Sensors and Their Potential Applications: A Review. *Adv. Funct. Mater.* **2016**, in press.
- (11) Takei, K.; Honda, W.; Harada, S.; Arie, T.; Akita, S. Toward Flexible and Wearable Human-Interactive Health-Monitoring Devices. *Adv. Healthcare Mater.* **2015**, *4*, 487–500.
- (12) Liu, Z.; Qi, D.; Guo, P.; Liu, Y.; Zhu, B.; Yang, H.; Liu, Y.; Li, B.; Zhang, C.; Yu, J. Thickness-Gradient Films for High Gauge Factor Stretchable Strain Sensors. *Adv. Mater.* **2015**, *27*, 6230–6237.
- (13) Yamada, T.; Hayamizu, Y.; Yamamoto, Y.; Yomogida, Y.; Izadi-Najafabadi, A.; Futaba, D. N.; Hata, K. A Stretchable Carbon Nanotube Strain Sensor for Human-Motion Detection. *Nat. Nanotechnol.* **2011**, *6*, 296–301.
- (14) McEvoy, M.; Correll, N. Materials That Couple Sensing, Actuation, Computation, and Communication. *Science* **2015**, *347*, 1261689.
- (15) Majidi, C. Soft Robotics: A Perspective—Current Trends and Prospects for the Future. *Soft Robotics* **2014**, *1*, 5–11.
- (16) Gong, S.; Lai, D. T.; Su, B.; Si, K. J.; Ma, Z.; Yap, L. W.; Guo, P.; Cheng, W. Highly Stretchy Black Gold E-Skin Nanopatches as Highly Sensitive Wearable Biomedical Sensors. *Adv. Electron. Mater.* **2015**, *1*, 1400063.
- (17) Gong, S.; Lai, D.; Wang, Y.; Yap, L. W.; Si, K. J.; Shi, Q.; Jason, N. N.; Sridhar, T.; Uddin, H.; Cheng, W. Tattoo-Like Polyaniline Microparticle-Doped Gold Nanowire Patches as Highly Durable Wearable Sensors. *ACS Appl. Mater. Interfaces* **2015**, *7*, 19700–19708.
- (18) Xu, S.; Zhang, Y.; Jia, L.; Mathewson, K. E.; Jang, K.-I.; Kim, J.; Fu, H.; Huang, X.; Chava, P.; Wang, R. Soft Microfluidic Assemblies of Sensors, Circuits, and Radios for the Skin. *Science* **2014**, *344*, 70–74.
- (19) Boland, C. S.; Khan, U.; Backes, C.; O'Neill, A.; McCauley, J.; Duane, S.; Shanker, R.; Liu, Y.; Jurewicz, I.; Dalton, A. B. Sensitive, High-Strain, High-Rate Bodily Motion Sensors based on Graphene-Rubber Composites. *ACS Nano* **2014**, *8*, 8819–8830.
- (20) Jeong, Y. R.; Park, H.; Jin, S. W.; Hong, S. Y.; Lee, S. S.; Ha, J. S. Highly Stretchable and Sensitive Strain Sensors using Fragmentized Graphene Foam. *Adv. Funct. Mater.* **2015**, *25*, 4228–4236.
- (21) Yan, C.; Wang, J.; Kang, W.; Cui, M.; Wang, X.; Foo, C. Y.; Chee, K. J.; Lee, P. S. Highly Stretchable Piezoresistive Graphene-Nanocellulose Nanopaper for Strain Sensors. *Adv. Mater.* **2014**, *26*, 2022–2027.
- (22) Kang, D.; Pikhitsa, P. V.; Choi, Y. W.; Lee, C.; Shin, S. S.; Piao, L.; Park, B.; Suh, K.-Y.; Kim, T.-i.; Choi, M. Ultrasensitive Mechanical Crack-based Sensor Inspired by the Spider Sensory System. *Nature* **2014**, *516*, 222–226.
- (23) Cheng, Y.; Wang, R.; Sun, J.; Gao, L. A Stretchable and Highly Sensitive Graphene-Based Fiber for Sensing Tensile Strain, Bending, and Torsion. *Adv. Mater.* **2015**, *27*, 7365.
- (24) Xiao, X.; Yuan, L.; Zhong, J.; Ding, T.; Liu, Y.; Cai, Z.; Rong, Y.; Han, H.; Zhou, J.; Wang, Z. L. High-Strain Sensors Based on ZnO Nanowire/Polystyrene Hybridized Flexible Films. *Adv. Mater.* **2011**, *23*, 5440–5444.
- (25) Souri, H.; Nam, I.; Lee, H. Electrical Properties and Piezoresistive Evaluation of Polyurethane-based Composites with Carbon Nano-Materials. *Compos. Sci. Technol.* **2015**, *121*, 41–48.
- (26) Li, X.; Zhang, R.; Yu, W.; Wang, K.; Wei, J.; Wu, D.; Cao, A.; Li, Z.; Cheng, Y.; Zheng, Q. Stretchable and Highly Sensitive Graphene-Polymer Strain Sensors. *Sci. Rep.* **2012**, *2*, 870.
- (27) Wang, Y.; Wang, L.; Yang, T.; Li, X.; Zang, X.; Zhu, M.; Wang, K.; Wu, D.; Zhu, H. Wearable and Highly Sensitive Graphene Strain

- Sensors for Human Motion Monitoring. *Adv. Funct. Mater.* **2014**, *24*, 4666–4670.
- (28) Kim, B. C.; Matsuoka, T.; Moraes, C.; Huang, J.; Thouless, M.; Takayama, S. Guided Fracture of Films on Soft Substrates to Create Micro/Nano-Feature Arrays with Controlled Periodicity. *Sci. Rep.* **2013**, *3*, 3027.
- (29) Nam, K. H.; Park, I. H.; Ko, S. H. Patterning by Controlled Cracking. *Nature* **2012**, *485*, 221–224.
- (30) Vandeparre, H.; Liu, Q.; Mineev, I. R.; Suo, Z.; Lacour, S. P. Localization of Folds and Cracks in Thin Metal Films Coated on Flexible Elastomer Foams. *Adv. Mater.* **2013**, *25*, 3117–3121.
- (31) Collaud Coen, M. C.; Lehmann, R.; Groening, P.; Schlapbach, L. Modification of the Micro- and Nanotopography of Several Polymers by Plasma Treatments. *Appl. Surf. Sci.* **2003**, *207*, 276–286.
- (32) Genzer, J.; Groenewold, J. Soft Matter with Hard Skin: From Skin Wrinkles to Templating and Material Characterization. *Soft Matter* **2006**, *2*, 310–323.
- (33) Lee, J.; Kim, S.; Lee, J.; Yang, D.; Park, B. C.; Ryu, S.; Park, I. A Stretchable Strain Sensor based on a Metal Nanoparticle Thin Film for Human Motion Detection. *Nanoscale* **2014**, *6*, 11932–11939.
- (34) Mattmann, C.; Clemens, F.; Tröster, G. Sensor for Measuring Strain in Textile. *Sensors* **2008**, *8*, 3719–3732.
- (35) Liao, X.; Liao, Q.; Yan, X.; Liang, Q.; Si, H.; Li, M.; Wu, H.; Cao, S.; Zhang, Y. Flexible and Highly Sensitive Strain Sensors Fabricated by Pencil Drawn for Wearable Monitor. *Adv. Funct. Mater.* **2015**, *25*, 2395–2401.
- (36) Lin, C.-W.; Zhao, Z.; Kim, J.; Huang, J. Pencil Drawn Strain Gauges and Chemiresistors on Paper. *Sci. Rep.* **2014**, *4*, 3812.
- (37) Wei, Y.; Chen, S.; Li, F.; Lin, Y.; Zhang, Y.; Liu, L. Highly Stable and Sensitive Paper based Bending Sensor using Silver Nanowires/Layered Double Hydroxides Hybrids. *ACS Appl. Mater. Interfaces* **2015**, *7*, 14182–14191.
- (38) Hwang, B.-U.; Lee, J.-H.; Trung, T. Q.; Roh, E.; Kim, D.-I.; Kim, S.-W.; Lee, N.-E. Transparent Stretchable Self-Powered Patchable Sensor Platform with Ultrasensitive Recognition of Human Activities. *ACS Nano* **2015**, *9*, 8801–8810.
- (39) Roh, E.; Hwang, B.-U.; Kim, D.; Kim, B.-Y.; Lee, N.-E. Stretchable, Transparent, Ultrasensitive, and Patchable Strain Sensor for Human–Machine Interfaces Comprising a Nanohybrid of Carbon Nanotubes and Conductive Elastomers. *ACS Nano* **2015**, *9*, 6252–6261.
- (40) Souri, H.; Nam, I.; Lee, H. A Zinc Oxide/Polyurethane-based Generator Composite as a Self-Powered Sensor for Traffic Flow Monitoring. *Compos. Struct.* **2015**, *134*, 579–586.
- (41) Gullapalli, H.; Vemuru, V. S.; Kumar, A.; Botello-Mendez, A.; Vajtai, R.; Terrones, M.; Nagarajiah, S.; Ajayan, P. M. Flexible Piezoelectric ZnO–Paper Nanocomposite Strain Sensor. *Small* **2010**, *6*, 1641–1646.
- (42) Gong, S.; Schwalb, W.; Wang, Y.; Chen, Y.; Tang, Y.; Si, J.; Shirinzadeh, B.; Cheng, W. A Wearable and Highly Sensitive Pressure Sensor with Ultrathin Gold Nanowires. *Nat. Commun.* **2014**, *5*, 4132.
- (43) Pang, C.; Koo, J. H.; Nguyen, A.; Caves, J. M.; Kim, M. G.; Chortos, A.; Kim, K.; Wang, P. J.; Tok, J. B. H.; Bao, Z. Highly Skin-Conformal Microhair Sensor for Pulse Signal Amplification. *Adv. Mater.* **2015**, *27*, 634–640.
- (44) Mannsfeld, S. C.; Tee, B. C.; Stoltenberg, R. M.; Chen, C. V. H.; Barman, S.; Muir, B. V.; Sokolov, A. N.; Reese, C.; Bao, Z. Highly Sensitive Flexible Pressure Sensors with Microstructured Rubber Dielectric Layers. *Nat. Mater.* **2010**, *9*, 859–864.
- (45) Yao, S.; Zhu, Y. Wearable Multifunctional Sensors using Printed Stretchable Conductors Made of Silver Nanowires. *Nanoscale* **2014**, *6*, 2345–2352.
- (46) Glass, P.; Chung, H.; Washburn, N. R.; Sitti, M. Enhanced Reversible Adhesion of Dopamine Methacrylamide-Coated Elastomer Microfibrillar Structures under Wet Conditions. *Langmuir* **2009**, *25*, 6607–6612.
- (47) Kim, S.; Sitti, M. Biologically Inspired Polymer Microfibers with Spatulate Tips as Repeatable Fibrillar Adhesives. *Appl. Phys. Lett.* **2006**, *89*, 261911.
- (48) Murphy, M. P.; Aksak, B.; Sitti, M. Gecko-Inspired Directional and Controllable Adhesion. *Small* **2009**, *5*, 170–175.
- (49) Sitti, M.; Fearing, R. S. Synthetic Gecko Foot-Hair Micro/Nano-Structures as Dry Adhesives. *J. Adhes. Sci. Technol.* **2003**, *17*, 1055–1073.
- (50) Park, J. J.; Hyun, W. J.; Mun, S. C.; Park, Y. T.; Park, O. O. Highly Stretchable and Wearable Graphene Strain Sensors with Controllable Sensitivity for Human Motion Monitoring. *ACS Appl. Mater. Interfaces* **2015**, *7*, 6317–6324.
- (51) Hempel, M.; Nezich, D.; Kong, J.; Hofmann, M. A Novel Class of Strain Gauges based on Layered Percolative Films of 2d Materials. *Nano Lett.* **2012**, *12*, 5714–5718.
- (52) Kong, J.-H.; Jang, N.-S.; Kim, S.-H.; Kim, J.-M. Simple and Rapid Micropatterning of Conductive Carbon Composites and Its Application to Elastic Strain Sensors. *Carbon* **2014**, *77*, 199–207.